METHODOLOGY DEVELOPMENT FOR THE AERODYNAMIC CENTER DETERMINATION OF THE ITA's UNMANNED AIRCRAFT VEHICLE WING-FUSELAGE CONFIGURATION

Roberto da Mota Girardi
Instituto Tecnológico de Aeronáutica (ITA). Praça Mal. Eduardo Gomes, 50, S J Campos – SP, Brasil
girardi@ita.br

André Valdetaro Gomes Cavalieri
Instituto Tecnológico de Aeronáutica (ITA). Praça Mal. Eduardo Gomes, 50, S J Campos – SP, Brasil
andre@ita.br

Tiago Barbosa de Araújo
Instituto Tecnológico de Aeronáutica (ITA). Praça Mal. Eduardo Gomes, 50, S J Campos – SP, Brasil
araujotb@ita.br

Abstract. *The unmanned aircraft vehicle (UAV) considered in this work has the specific mission of examining elements of an electric energy transmission line (the tower, vegetation at the neighbor area and the electric cables). Such aircraft has some particular characteristics: (i) a relatively small velocity, that is, low Reynolds number, (ii) different material and manufacturing techniques are used and (iii) the weight is very low and, therefore, the aircraft will be very sensitive to atmospheric gusts. Such characteristic increases the difficulty to accomplish the mission, that is, performing a pre-defined path along a transmission line and its elements imaging. One of the most important parameters to allow aircraft stability is the aerodynamic center position (Xca), defined as the position where the aircraft pitch moment do not vary with the angle of attack. In the classical methodology used during the conceptual design phase, the mayjor error source is the determination method used to obtain the Xca displacement due to the fuselage submited to the flow field generated by the aircraft wing. Using experiments and simple numerical tools, an improved methodology will be developed in order to be used in future UAV developments. The experiments will be performed at the ITA's Wind tunnel and half models will be used.*

Keywords*: Unmanned Aircraft Vehicle, wing-fuselage configuration, Experimental and Numerical Methods, Aerodynamic center determination*

1. INTRODUCTION

Unmanned aircraft vehicles (UAV) can be used in several civil applications, like that: (i) Electrical lines and pipelines examination, (ii) harbors, forest reservations and less accessible frontiers vigilance, (iii) aircraft and disappeared people rescue, (iv) aerial picture generation and (v) others.

In 2004 Technological Institute of Aeronautics (ITA) was contacted to participate in a cooperation involving Advanced System Studies Center of Recife (CESAR) and São Francisco Electric Company (CHESF). The goal of such cooperation was an UAV development, for electrical line elements (towers, vegetation existing in the neighborhood of electrical lines, electrical connectors at the towers and etc) examination. In order to accomplish this task, a very low velocity (80 km/h) aircraft, flying at low altitude, is required, due to infrared camera limitations (required to observe hot spots, which indicate electric problems at some line elements). In such velocity range, atmospheric gusts became very important due to these effects on the flight security and because the electric line elements examination mission became very difficult, due the constant aircraft attitude changes.

The low aircraft velocity, required to accomplish the infrared camera examination mission, is in the inferior limit of an airplane flight envelope, because a high wing loading (W/S) is necessary to give the aircraft a low sensibility to atmospheric gusts, but, on the other hand, a low value of W/S is required to accomplish the low velocity flight requirement. All mission requirements could be fulfilled by using other kinds of aircrafts, like a helicopter, a dirigible or a hybrid vehicle, that is, a mixture between a dirigible and an airplane, for example. The most adapted kind of aircraft was analyzed by Girardi and Rizzi (2005a), where an airplane was chosen to be the kind of aircraft used in this project.

The second step in the conceptual phase of the airplane project was the definition of the more adapted configuration, considering all requirements fulfillment. Two basic airplane configurations were considered: (i) in the first one the engine is located at the airplane nose, a conventional tail was chosen to give stability and control to the aircraft and the camera was located at the fuselage low surface, near the aircraft gravity center (GC). (ii) In the second configuration, the engine was located at the fuselage tail, in the pusher configuration, and two booms were used to assembly the tail to the wing. In this configuration, the camera could be located at the fuselage nose or in the same place of the first configuration. Both configurations have high wing position (relative to the fuselage), a tricycle landing gear

type and a rectangular wing. These configurations were analyzed by Girardi and Rizzi, (2005b) and the first one was chosen, considering the camera position near the aircraft GC (better to decrease effects on the camera due to the aircraft constant attitude changes, associated to the gusts effects) and the design team experience.

The aircraft conceptual design phase was executed by the Aeronautics Department of ITA and a special methodology was developed (Girardi e Rizzi, 2006) to face the problems associated to the airplane specific mission, that is, image acquisition from an aircraft at low velocity, manufactured with non conventional material and subjected to atmospheric gusts, because of the low altitude required by the infrared imaging. In such methodology, the aircraft dimensions were determined considering the autopilot characteristics and this is an important aspect of the procedure adopted to this UAV design.

The work reported in this paper is inserted into the preliminary design phase, where more accurate information has to be used in order to improve the analysis methods used to determine the airplane dimensions, as well as, the relative positions of the different aircraft parts (wing, fuselage and tail). One of the problems verified during the conceptual design phase was the lack of information on low Reynolds number aerodynamic data, required to a small vehicle at low velocity. Such kind of information is very useful to generate the aircraft characteristic curves (CL x α, CL x Cm and the drag polar), which are used to performance, as well as, stability and control calculations.

During the aircraft design conceptual phase, the aerodynamic characteristics of the complete configuration, that is, wing, fuselage and tail, are generated by using a semi-empirical methodology (Roskam, 2000-2003, and Raymer, 1999), where fuselage is considered a body of revolution and the airplane parts interference are calculated by using empirical factors, which do not consider the actual way the aircraft parts are joined together. It is important to note that such factors were obtained to full scale airplanes, where Reynolds number is high.

The actual UAV fuselage is not a body of revolution. It has a rectangular cross section and, along its length, it is constituted by: (i) a small nose, containing the engine and its support, (ii) a constant cross section area part, where fuel tank, parachute, cameras, electronic equipment for guidance and control and batteries are installed and, finally, (iii) a trailing cone, characterized by a cross section area reduction, performed with the lower surface inclination. The upper trailing cone surface is in the same plane of the constant cross section area part of the fuselage. In such kind of fuselage, longitudinal vortices can be generated due to the abrupt area variation at the trailing cone interface, resulting induced drag and lift variations. The wing is positioned at the fuselage upper surface and flow interference can be observed at the corner formed by the union of these aircraft parts.

The objective of this paper is to present experimental results to the aerodynamic characteristic curves of the UAV wing-fuselage configuration, at low Reynolds number. The experiments were performed in an open circuit wind tunnel and a three component balance was used to obtain lift, drag and pitch moment of a half model (balance is assembled at the wind tunnel lateral wall). Wool tufts were used to allow flow visualization of the model at several angles of attack, in order to generate information to perform experimental result analysis. The questions discussed above are considered during the experimental results analysis and the aerodynamic center is obtained directly from the results.

Finally, the experimental results are compared with the semi-empirical methodology mentioned above to verify its applicability to the specific fuselage used for the UAV developed at ITA. This comparison allows modification of the semi-empirical method and, therefore, more reliable aerodynamic characteristic curves could be generated to future fuselage, with similar shape and subjected to a flow with similar Reynolds number.

2 EXPERIMENTAL APPARATUS

The measurements were performed in a blower wind tunnel with square test section, characterized by a dimension of 460 mm. The flow velocity ranges from 4 to 30 m/s and the turbulence intensity is 0.5% at the maximum velocity. Along the test section length the cross section area is changed in order to compensate the boundary-layer growth and, as a consequence, to keep a constant static pressure. This area change is performed by filling the test section corners with triangular elements, whose dimension changes along test section length, as shown in the Fig. X.

Lift, drag and pitch moment of a model are measured with a balance fixed at the test section lateral wall (outside the wind tunnel). Aerodynamic forces and moment on the model are transmitted to the balance through a metal axis. Such balance has a triangular plate used to fix the metal axis originated at the model. The triangular plate is connected to the wind tunnel structure by using three load cells (metal plates, instrumented with four strain gages each, in order to assembly a complete Wheatstone bridge). Two of these load cells are used to make measurement of lift and pitch moment (sensors A and F) and the third one is used to obtain drag force measurements (sensor D). Each load cell is connected to an independent signal conditioner module (amplifier and filter), which allows adjustment of the output voltage considering the data acquisition board characteristics. For the present experiment, the maximum output voltage of each sensor is chosen to be 10 volts, which maximize measurements resolution.

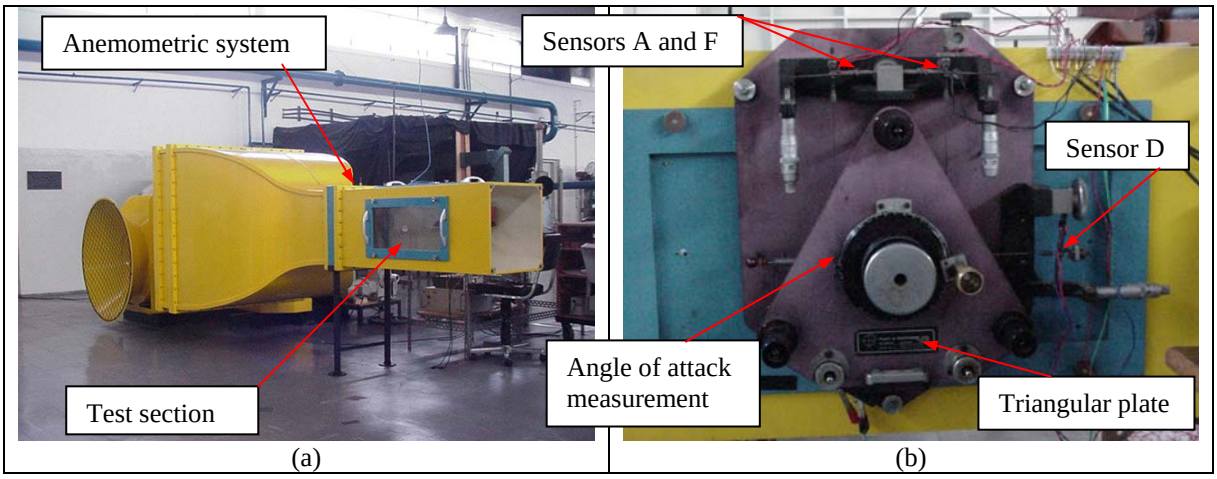

Figure 1: (a) Open circuit wind tunnel and (b) three component aerodynamic balance.

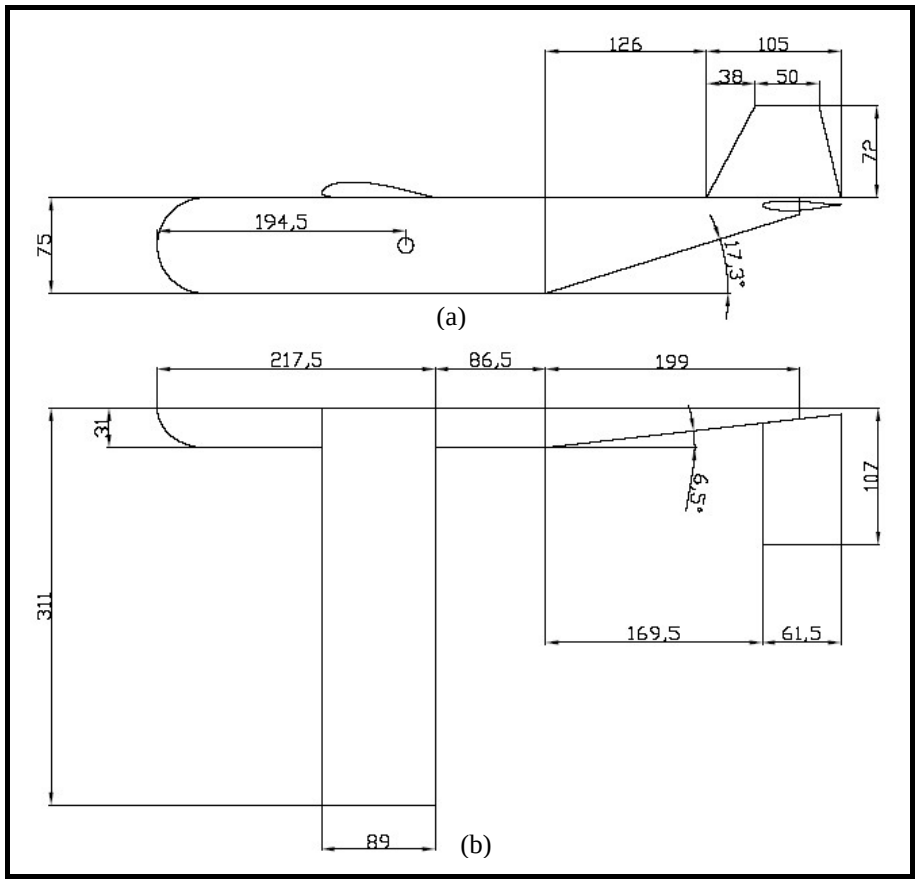

Figure 2: Half model of the complete configuration: (a) Lateral view and (b) plan view . Dimensions in mm.

The dynamic and static pressures are measured by using a Pitot tube located at the beginning of the test section (tunnel anemometric system), just after the end of the contraction section, as can be seen in the figure 1(a). Pressure transducers are connected to the Pitot tube and a signal conditioner is used to amplify the output voltages before the connection with the data acquisition board.

The model angle of attack is varied manually and its measurement is performed by a rotating device (where the model axis is fixed) divided in 360 equal parts. The uncertainty of ± 0.5 degrees can be considered to this measurement.

Due to the balance configuration, the aerodynamic tests have to be performed with a half model, as shown in the figure 2. The wing-fuselage configuration model was manufactured with wood (see Fig. 3a) and it has the following characteristics: (i) a fuselage with a small nose region, a constant rectangular cross section part, with 75 mm high and 31 mm width and a trailing cone, where the cross section area decreases along the model longitudinal axis, (ii) a rectangular wing with aspect ratio equal to 7. A Selig SD7062 airfoil is used and the wing is positioned at the fuselage upper surface, with 2.4 degrees incidence angle. (iii) Landing gears were not considered in the present tests. The model

is 503 mm total length and a steel axis is fixed at 194,5 mm from the model nose and it is used to fix the model to the aerodynamic balance. The fuselage frontal area is 0.0023 m^2. Considering the test section cross section area, the model blockage ratio is approximately 1,1% and, therefore, the test section walls interference on the model flow is very low.

For half model testes, the model symmetrical plane (wind tunnel wall) should be a flow stream plane and the wall boundary layer flow should be eliminated to accomplish rigorously such requirement. One end plate (see Fig. 3) is used to isolate the wind tunnel boundary layer from the flow over the fuselage model, in order to approximate the flow over the model to the free flight flow. The experimental results reported by Kubo (1989), were used, initially, to define the end plates dimensions. The distance the end plate is fixed from the wind tunnel lateral wall is defined as a function of the boundary layer thickness, determined in a previous work by using a hot wire anemometer.

After experiments conducted with an airfoil model, a flow field between the two sides of the end plates was observed, generating longitudinal vortices along the upper and lower edges of the end plate and causing great disturbances on the model flow. Such problem is discussed in Girardi et alli (2007) and the problem was solved with an end plate spanning the test section high (see Fig. 3b), to avoid flow communication through the upper and lower edges of the end plate. The same end plate configuration was used in the present work.

(a) (b)

Figure 3: (a) Wing-fuselage half model assembled at the wind tunnel (b) rear view of the model inside the wind tunnel test section.

3. EXPERIMENTAL PROCEDURE

In the present work, the following measurements have to be performed: (i) the forces and pitch moment of the complete model configuration, (ii) the dynamic pressure, necessary to obtain the non-dimensional coefficients for lift (Cl), drag (Cd) and pitch moment (Cm). In this paper section, the experimental procedure established to determine each one of the above parameters is described, in order to show all care taken to guarantee reliable results.

As mentioned in the preceding section, lift, drag and pitch moment are measured by using an aerodynamic balance, with three load cells. The first task to be done is the load cells calibration, in order to obtain a correlation between the force acting on each load cell with the voltage read by the acquisition system. The calibration procedure is performed by incrementing loads from zero to the maximum value estimated for the specific sensor of the balance and, after that, a decrement is done up to zero again. At least 20 measures are used for the calibration process, in order to determine statistic parameters, used to uncertainties estimates. During such procedure, a small amount of vibration is used to decrease the time required to the balance structural parts accommodation and it is worth to note that such vibration is kept during the sampling process, performed by the data acquisition system. In the calibration procedure, one thousand measures were performed during a sampling time of one second and just a value (average of 1000) of voltage is correlated to the force imposed on the load cell. Each balance sensor is loaded by using calibrated masses and a system constituted by cables and pulleys, responsible to apply the force to an axis connected to the balance, as can be seen in the figure X. The three balance sensors are calibrated in two steps: (i) the load cell associated to the drag force is calibrated alone but (ii) for the other two sensors, the vertical load applied to the axis connected to the balance is divided by two and the load cells associated to the lift and pitch moment are calibrated simultaneously.

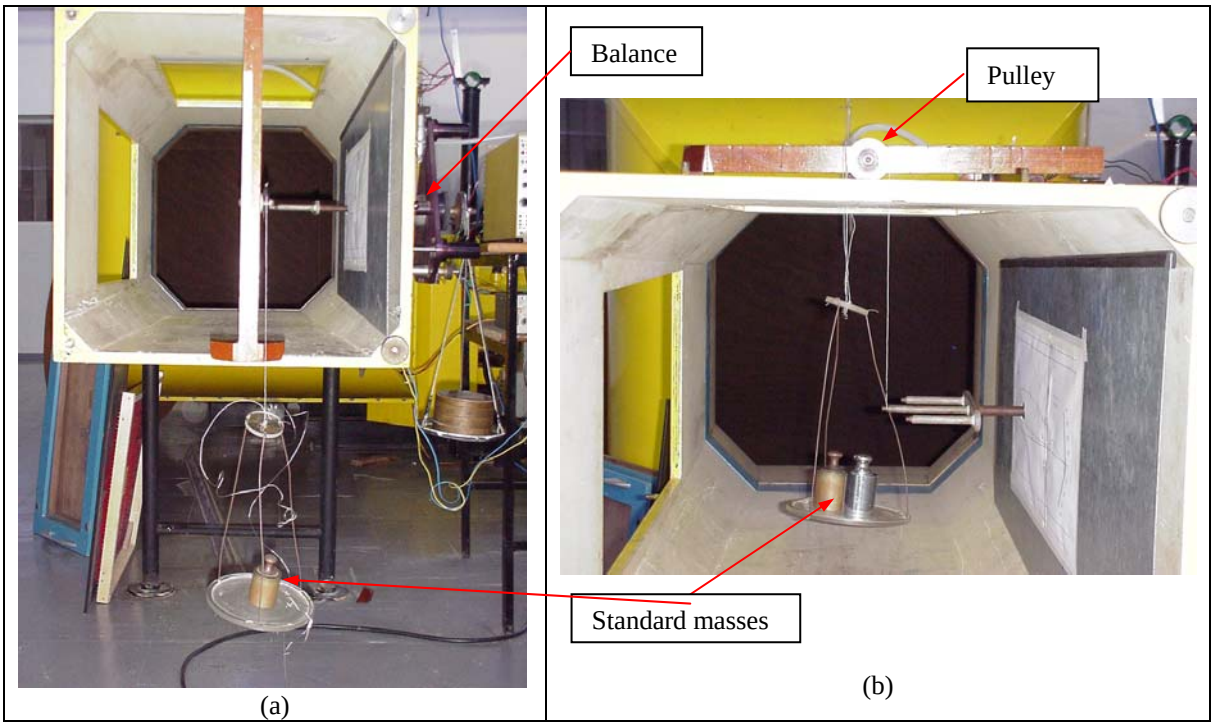

Figure 4: Aerodynamic balance calibration apparatus: (a) drag sensor and (b) Two other sensors used to obtain lift and pitch moment.

At the region where anemometric system is located (at the beginning of the test section) the flow field is distorted, due to the area variation along the contraction, causing errors in the values measured for the dynamic and static pressures. This problem can be corrected by performing a calibration procedure, where a Pitot tube, placed at the test section central region (location where models are tested) is compared with the anemometric system fixed at the wind tunnel. Calibration curves for the dynamic and static pressures are the results of the above procedure and they are used to correct the experimental results obtained with the wind tunnel anemometric system (The Pitot tube at the test section central region is withdrawn during the model experiments). The above calibration curves are incorporated in a computer code used to make calculations of the aerodynamic coefficients.

As mentioned in the previous section, the dynamic pressure is measured by using a pressure transducer, ranging from zero to 100 mm of water. A Betz manometer, with least count of 0,1 mm of water, is used as standard for the pressure transducer calibration, which is performed in the following way: (i) Initially, the pressure is increased and decreased several times (minimum of three) in order to get a repeatable measure of zero gage pressure at the Betz manometer. With such procedure, the internal walls of the Betz manometer are wetted. (ii) Starting from zero, the pressure is increased up to 50 mm of water, in steps of 5 mm and then (iii) pressure is decreased, using the same steps, up to zero again. For each point of the calibration curve, one thousand measures are collected during one second after the pressure stabilization (observed at the Betz manometer). The data acquisition code, written in LabView ambient, presents the linear fit of the experimental data and the standard deviations associated with the uncontrolled parameters of the experimental setup (random errors). These parameters are used to estimate the uncertainties associated to the aerodynamic coefficients.

After the calibration phase was finished, the experiment can be run in the following manner: (i) the end plate is assembled inside the wind tunnel test section, whose longitudinal axis is stamped on the end plate surface in order to allow model alignment. (ii) The model is fixed to the wind tunnel aerodynamic balance (through its metal axis) and initial alignment is performed, comparing the fuselage model upper surface with the longitudinal axis stamped on the end plate surface. (iii) Before starting the wind tunnel, all sensor signals are read by the data acquisition system (initial voltages). This operation is performed after some vibration was introduced, in a similar manner used during the aerodynamic balance calibration (see preceding section), in order to guarantee all load cells are well accommodated to the loads associated the zero dynamic pressure. The initial voltage accuracies are very important because all force measurements accuracies depend on them. It is worth to note that the aerodynamic forces and moments are obtained through the difference between the sensor signal (voltage), measured with wind tunnel turned on, and the initial voltage (obtained with flow velocity equal to zero). (iv) In the next step, wind tunnel is turned on and the dynamic pressure required to the specific test is established. (v) The following results are typically obtained in an aerodynamic test program: The drag polar (Cd x CL), Cl x α and Cm x α. With the dynamic pressure fixed at a required value (associated to the Reynolds number) the angle of attack (α) is varied. In general, such variation starts at a negative angle of attack

and increments of 1 degree are used. (vi) During the experiments described above, a data acquisition code, written in the LabView ambient, is used to make the measurements of the aerodynamic balance sensors (three) and the pressure transducer, used to register the wind tunnel dynamic pressure. For each angle of attack, whose value is inserted through the keyboard, the four sensor signals, are sampled 2000 times, using sampling rate of 200 hz. The resulting sample time of 10 seconds was chosen to account for the wind tunnel dynamic pressure variations and an average value is obtained for each parameter measured in this experiment. (vii) Data reduction is performed with other computational code, written in the LabView ambient, where the data generated to each sensor (voltages) is combined with the calibration curves to determine forces and moments acting on the model. Ambient pressure and temperature are used to calculate air density and dynamic viscosity. These parameters are combined with the dynamic pressure to calculate the test Reynolds number. Finally, the model reference area (wing area) together with the forces and moments are used to determine the aerodynamic coefficients mentioned previously.

Data generated during calibration procedure, as well as, during the experiment are used to determine the uncertainty associated to each aerodynamic coefficient. The uncertainty analysis was made by using the procedure described by kline and Mcintoch (1953).

4. ANALYSIS OF RESULTS

According to the preceding sections of this paper, measurements were taken using an aerodynamic balance, which measure the lift, drag and pitch moment of the half model engaged on it. This was made for three different Reynolds number (Re) varying the angle of attack (α) in a wide range, in which we can check the linear behavior of the lift coefficient, in the interesting range, before stalling as we can see at figure 5. The Re numbers used in these experiments are relatively low, but they are near the cruise flight number.

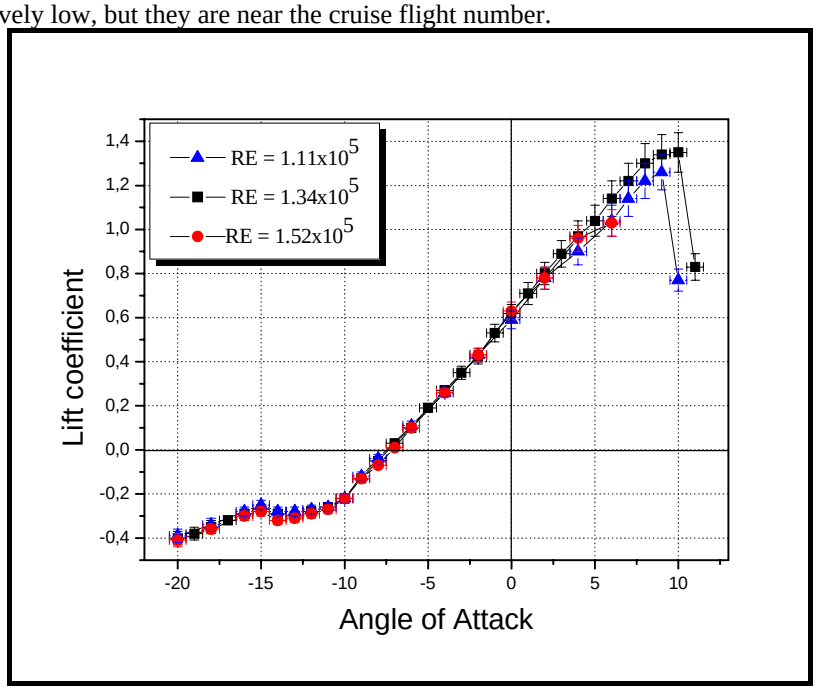

Figure 5 – Lift coefficient variation with the angle of attack.

The error bars indicated in the graphics of this paper were all made using a combination of the errors of each coefficient component. They are shown with the probability of 95%.

For the higher Re, measurements were just made until the stall angle, which is the interesting region for the aerodynamic center determination. We can note from this graphic that the Reynolds number variation don't have much influence in the linear range, where we are interested. The changing in Re just alter the maximum lift coefficient as we hold. This cannot be confirmed, as we said before, for the higher Re because we didn't get the stall angle for this.

Using the semi-empirical method (see Roskam, 2000-2003), the linear part of the lift coefficient (Cl) and the maximum value for Cl, as well as, the angle of attack for Cl_{max} was estimated for the configuration tested in this paper. These results are compared in the table 1. The maximum value of the lift coefficient, as well as, the angle of attack, where the wing stalls, were calculated by using, the so called, critical section method. In such method, the lift coefficient distribution along the wing span is calculated for several values of angle of attack, by using the vortex lattice method. The lift coefficient of each station along the wing span (Cl) is compared with the maximum lift coefficient (Cl_{max}) the airfoil placed at the station is capable to generate. The wing is considered stalled when the first station Cl is equal to Cl_{max} and the angle of attack associated to that Cl distribution along the span is considered the stall angle. In

general, this kind of method furnishes lower values for Cl_{max} and for the stall angle, because the wing stall actually occurs when several stations along the wing span are stalled. In table 1, the values obtained for Cl_{max} , with both methods, are in good agreement. The experimental value is lower than the theoretical one, probably because the fuselage is causing interference, reducing the wing alone maximum lift coefficient. The lift curve slope (Cl_α) has small variation as a function of Reynolds number. All the experimental values registered in the table 1 were obtained for the lower Reynolds number tested in the present work. The difference observed for the angle of attack where the wing stalls is a consequence of the differences for Cl_{max} and α_o.

Table 1: Lift coefficient parameters for the wing-fuselage configuration. Comparison between experiments and theoretical estimates

Approach	α_o	(Cl_α)	(Cl_{max})	α for Cl_{max}
Experiments	-7.0	0.0788	1.25	8.5
Semi-empirical method	-6.4	0.0781	1.30	10.2

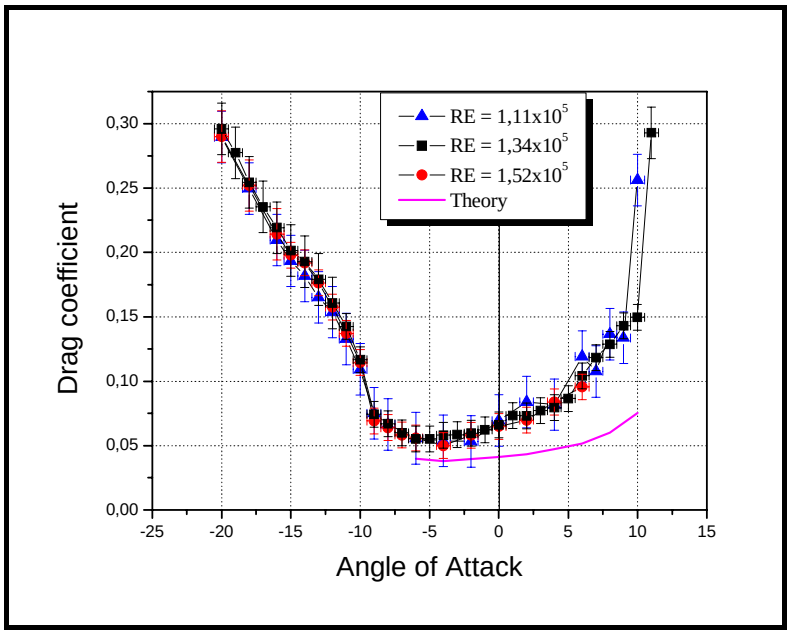

Figure 6 – Drag coefficient for the wing-fuselage configuration as a function of the angle of attack

The drag coefficient as a function of the angle of attack is presented in the Fig. 6. Together with the experimental results is shown a theoretical curve, obtained by a semi-empirical methodology describe bellow: Initially, the wing alone drag coefficient was estimated by using the lift coefficient distribution along the wing span (obtained by using the vortex lattice method) for an angle of attack value. Using the airfoil experimental drag polar, the wing drag coefficient was determined through integration of the Cd along the wing span. The wing drag coefficient as a function of angle of attack is obtained by repeating the above calculation for a set of α values. The experimental drag coefficient for the fuselage, with rounded corner (see Girardi et alli, 2007), was added to the wing Cd estimates, considering the wing incidence angle is 2.4 degrees, in order to obtain the wing-fuselage drag, where no interference was considered.

When experiments and theory (described above) are compared (see Fig. 6) a significant interference between wing and fuselage is detected and it is increased with the angle of attack. This interference is caused by longitudinal vortices generated at the interface between the wing lower surface and the fuselage lateral surface. Other source of interference is the flow separation caused in the flow over the fuselage upper surface, due to the wing presence. Such interference can be minimized by using streamlined surfaces.

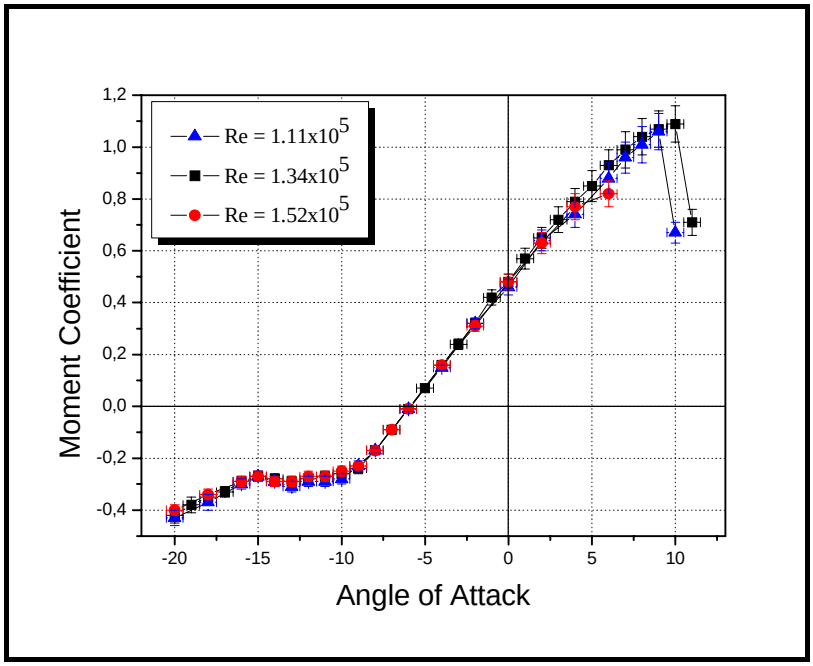

Figure 7 – Moment coefficient at model axis for the wing-fuselage configuration.

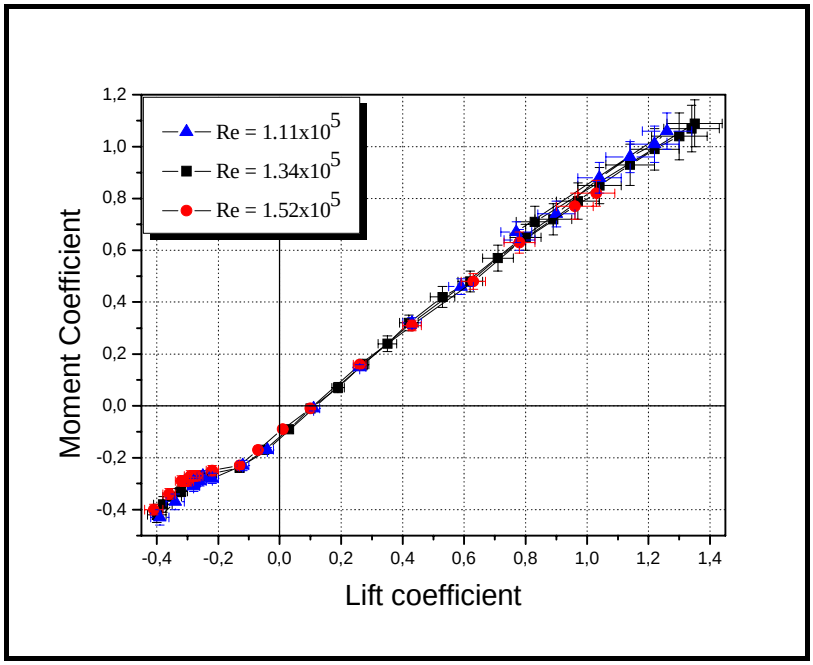

Figure 8 - Moment coefficient about the model axis against lift coefficient.

The pitch moment coefficient as a function of angle of attack is shown in figure 7, wherein it was set at model axis, whose position is shown at Fig. 2. For this configuration the axis is behind the quarter chord of the wing and the configuration aerodynamic center is ahead of this position, because fuselage has this effect on the aerodynamic center position. Due to this, the stability coefficient $\frac{dC_M}{d\alpha}$ is positive and this is compatible with the static margin considered the model axis as the configuration gravity center.

The mayor objective of the present work is to determine the configuration aerodynamic center, which can be obtained by using the equation:

$$\frac{X_{AC}}{c} = -\frac{dC_M}{dC_L} + \frac{X_{AXIS}}{c} \qquad (1)$$

Where the derivative coefficient of this equation can be obtained from the experimental slope determined in the region of linear variation of the moment coefficient as a function of C_L. Figure 8 shows the graphic of the moment coefficient about the model axis versus the lift coefficient.

From these curves we determined the experimental slope, which are shown in the table 2, where every slope is presented with the probability of 95%. Since $\frac{X_{AXIS}}{c}$ is constant and equal to $1.05 \pm 0.01 (2\sigma)$ (X-axis origin is located at the fuselage nose) we can easily calculate the aerodynamic center using the above equation (wing chord is used as characteristic dimension) and the results of the table 2. The values determined, as described before, are shown in the table 3 with the probability of 95%.

Table 2 – Experimental slopes for its respective Reynolds numbers.

Reynolds Number	Experimental Slope
$RE = 1.11 \times 10^5$	$0{,}94 \pm 0{,}02$
$RE = 1.34 \times 10^5$	$0{,}94 \pm 0{,}02$
$RE = 1.52 \times 10^5$	$0{,}93 \pm 0{,}02$

Table 3 – Aerodynamic Center position for the Reynolds Numbers used.

Reynolds Number	Aerodynamic Center Position
$RE = 1.11 \times 10^5$	0.11 ± 0.03
$RE = 1.34 \times 10^5$	0.11 ± 0.03
$RE = 1.52 \times 10^5$	0.12 ± 0.03

As we can see from the table 3, the position of the aerodynamic center for the configuration used are in the same range, but the uncertainty is more than 25% and this is not small when a 10% static margin is considered to an aircraft. Using the semi-empirical method described by Roskam (2000-2003), the aerodynamic center estimated is located at 15% From this we can say that the traditional methods for determining aerodynamic center used here, for wing-fuselage configurations gives good results for unmanned aircrafts.

Now with the aerodynamic center determined for the wing-fuselage configuration at each Re, we can sketch the moment coefficient about this point, what is shown in the figure 9 for the three Re specified. The pitch moment coefficient, around the aerodynamic center, should be constant for the linear range. The variations obtained for such parameter are justified by some non-linear behavior of the Cm x Cl curve, presented in the Fig. 8.

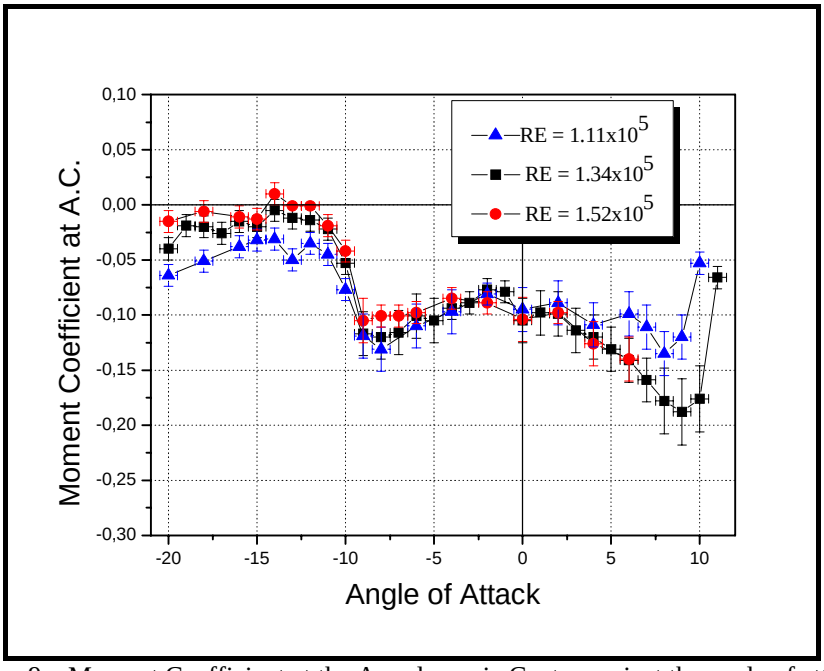

Figure 9 – Moment Coefficient at the Aerodynamic Center against the angle of attack.

We can see from the figure 9 that there is a narrow region where the moment coefficient is independent of the angle of attack. This is due to the fact that we don't have a real straight line in the graphic for the chosen profile of, as we can see at Fig. 8.

5. FINAL REMARKS

The lift curve estimated by the semi-empirical method and experimental results are in good agreement, showing the theoretical method is appropriated to be used in the UAV conceptual design.

The interference between wing and fuselage generates a drag increment, caused by the longitudinal vortices originated at the corners formed by the wing lower surface and the fuselage lateral surfaces. Other source of interference was the fuselage upper surface flow separation, caused by the wing obstruction. In future works, streamlined surfaces will be used to minimize the interference described above.

The wing-fuselage aerodynamic center position was one of the main objectives of the present paper, due to the uncertainty associated to the aerodynamic center displacement, caused by the fuselage subjected to the flow generated by the wing. The difference between the semi-empirical method and experimental one was 3% of the aerodynamic chord. Considering the airplane static margin is approximately 10% (typical value), the above difference is significant even more, considering the experimental value is closer to the airplane gravity center and, then, the aircraft could have stability problems.

Large aerodynamic center location uncertainty was obtained and must be reduced in future experimental works. The data obtained in the present work will be useful to improve the semi-empirical method used to aircraft design.

6. ACKNOWLEDGEMENTS

To the Financiadora de Estudos e Projetos (FINEP), for supporting part of the resources used to the Unmanned Aircraft Vehicle development (protocolo 243/2004) and to the Centro de Estudos de Sistemas Avançados do Recife (CESAR), to the partnership in this project. To the staff of the Prof. K.L. Feng Aeronautical Engineering Laboratory: Carlos Guedes Neto, Luis Zambrano Lara, Vitor Valentim Betti and Mario Correia.

7. REFERENCES

Bearman, P.W. (1965): Investigation of the flow behind a two-dimensional model with a blunt trailing edge and fitted with splitter plates. *J. Fluid Mech*., Vol. 28, pp. 241-255.

Girardi, R.M. e Rizzi, P., (2005a), "Análise do tipo da aeronave mais adaptada para a inspeção de linhas de transmissão", Relatório de Trabalho, CESAR/ITA, 27 de junho.

Girardi, R.M. e Rizzi, P., (2005b), "Seleção da alternativa mais promissora para prova de conceito, através da construção e testes em vôo", Relatório de Trabalho, CESAR/ITA, 27 de junho.

Girardi, R.M. e Rizzi, P., (2006), "Desenvolvimento de Metodologia para Projeto Conceitual de um Veículo Aéreo Não Tripulado (VANT), Usado para Inspeção de Linhas de Transmissão de Energia Elétrica", Anais do Congresso Nacional de Engenharia Mecânica (CONEM), Recife, Pe.

Girardi, R.M. e Rizzi, P., (2006), "Projeto Conceitual de um Veículo Aéreo Não tripulado, Usado para Inspeção de Linhas de Transmissão de Energia Elétrica". Anais do 11º Encontro Nacional de Ciências e Engenharia Térmicas (ENCIT 2006), Curitiba, Dez. 5-8.

Kline, S.J. and McClintock, F. A. (1953): Describing uncertainties in single-sample experiments. *Mechanical Eng*., pp. 3-8.

Kubo,Y. et all.(1989): Effects of end plates and blockage of structural members on drag forces. *J. Wind Eng. Ind. Aerodynamics*, vol.32, pp.329-342.

Rae, W.H. and Pope (1984), A *Low speed wind tunnel testing*. Second edition, John Wiley & Sons, USA.

Raymer, D.P., (1999), "Aircraft design: a conceptual approach", AIAA Education Series, AIAA, Washington DC.

Roskam, J., (2000-2003), "Airplane design", parts I-VIII, Dar Corporation, Lawrence, Kansas, USA.

8. RESPONSIBILITY NOTICE

The authors are the only responsible for the printed material included in this paper.